International Journal of Earth, Energy and Environmental Sciences
ISSN: 2517-942X
Vol:9, No:6, 2015

Material Flow Modeling in Friction Stir Welding of AA6061-T6 Alloy and Study of the Effect of Process Parameters

B. Saha Roy, T. Medhi, S. C. Saha

***Abstract*—**To understand the friction stir welding process, it is very important to know the nature of the material flow in and around the tool. The process is a combination of both thermal as well as mechanical work i.e. it is a coupled thermo-mechanical process. Numerical simulations are very much essential in order to obtain a complete knowledge of the process as well as the physics underlying it. In the present work a model based approach is adopted in order to study material flow. A thermo-mechanical based CFD model is developed using a Finite Element package, Comsol Multiphysics. The fluid flow analysis is done. The model simultaneously predicts shear strain fields, shear strain rates and shear stress over the entire workpiece for the given conditions. The flow fields generated by the streamline plot give an idea of the material flow. The variation of dynamic viscosity, velocity field and shear strain fields with various welding parameters is studied. Finally the result obtained from the above mentioned conditions is discussed elaborately and concluded.

***Keywords*—**AA6061-T6, friction stir welding, material flow, CFD modelling.

I. Introduction

THE Friction stir welding (FSW) technique was invented by The Welding Institute (TWI) [1] in 1991, and since then has become a significant joining technology. It is a solid-state joining process that uses a third body; a rotating tool to join two faying surfaces which are rigidly clamped to each other. The tool used is a non-consumable cylindrical shouldered one and having profiled pin. The tool shoulder is in contact with the work surface and the tool pin is slightly shorter than the weld depth required. Heat is generated as a result of friction between the tool and the material which results in severe plastic deformation and flow of this plasticized material takes place simultaneously as the tool moves along the length. The schematic diagram is as shown in Fig. 1.

During FSW, the material flow process is quite complex. The material flow is dependent on the tool geometry, process parameters and the material to be welded. Hence in order to obtain an optimal tool design and highly efficient welds it is very important to understand the material flow characteristics [3]. A physical model of the metal flow in the FSW process was given by [4] where the metal motion was described by kinematics which is also been followed by many other authors. A solid mechanics approach was followed by [5] considering a rigid visco-plastic material showing the dependence of flow stress on strain rate and temperature. Schmidt et al. [6] used adaptive boundary conditions to determine conditions for void-free welds using finite element analysis and flow stress determined according to the Johnson-Cook law. Buffa et al. [7] developed a thermo-mechanically coupled, rigid visco-plastic, three-dimensional finite-element model and studied the effect of tool geometry and welding velocity on material flow pattern and the grain size distribution in the welded joints. Also experimentally, optical microscopy, movement of tracer particles and spatial variations of texture have been used to understand material flow. Although, post weld characterization of the welds does not provide any direct information, the observations provide some indication of material flow in FSW. Steel balls have been used to trace flow in butt welds of 6061 and 7075 aluminium alloys [8], their positions after welding being determined using radiography. Another way to understand flow experimentally is to use inert markers before starting the weld [9], and then characterizing their final positions using serial sectioning parallel to the top surface. Schmidt et al. [10] estimated the average velocity of material flow through shear layers during FSW of aluminum alloy based on experimental investigation of tracer flow. The estimated average velocity was found to be approximately 0.1 to 0.3 times the shoulder rotational speed. The tracer technique does not provide information about the actual flow path of the material. It only shows the final position of the tracer.

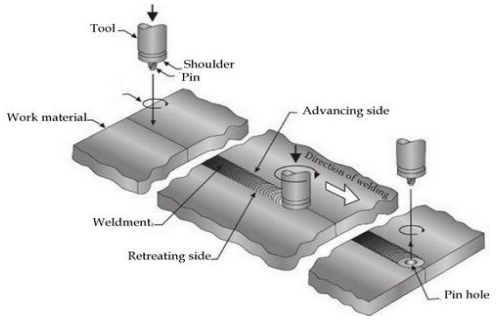

Fig. 1 Schematic diagram of friction stir welding process [2]

B. Saha Roy is with the Department of Mechanical Engineering as Assistant Professor in, National Institute of Technology, Agartala, India (Phone: +91-9612842102; e-mail: erbarnik@yahoo.co.in).

T. Medhi, Research Scholar, and S. C. Saha, Professor, are with the Department of Mechanical Engineering, National Institute of Technology, Agartala, India (e-mail: tanmoymedhi@gmail.com, subashchandrasaha@yahoo.in).

The objective of this research is to study material flow in the welded plate. The study is carried out by a model based approach to create the numerical flow model by using Comsol Multiphysics. Then the effect of the welding parameters namely the sticking condition, rotational speed and welding speed for friction stir welding (FSW) is quantified. The material flow conditions are incorporated in the model in order to study the material flow in and around the tool pin as well as the shoulder interface.

II. Present Investigation

From the previous section it is noticed that there are various flow models generated numerically for proper understanding of the material flow in FSW process. Many researchers have put forward their theories and findings about the material flow in and around the tool. To fulfil the current research objective, a process is followed which is essentially a model based approach to observe the material flow in FWS process. Finally the flow model which is developed will be used to simulate the process and the effect of various parameters on the material flow, viscosity, shear rate etc. will be studied.

A. Numerical Approach

The proposed modelling approach is a physics-based model which is based on understanding the principles by experiments and theory. The model was generated by Comsol Multiphysics Simulation Software which is very highly efficient in solving multiphysics based welding problems that are transient in nature and highly non- linear. The main aim of the model is to solve the governing equation and predict the nature of material flow in the regions surrounding the tool by varying the welding parameters. The temperature-dependent material properties as well as the contact condition are also considered in order to extend the FSW process modelling. A general representation of the model is shown in Fig. 2.

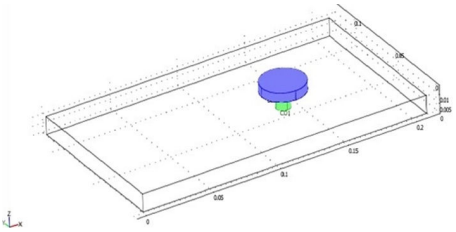

Fig. 2 General representation of the model, the shoulder is shown in green, the insert in violet and the plate is made transparent

The model geometry includes two, three-dimensional pieces in a Cartesian coordinate system, a tool and an aluminum plate. The tool is comprised of a shoulder 0.032 m diameter with a pin of 0.01 m diameter and 0.0095 m height extending down from the shoulder center as shown in Fig. 3.

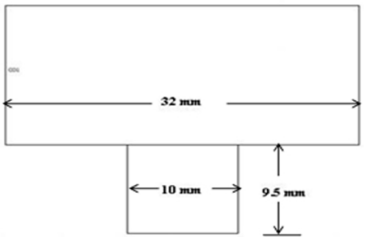

Fig. 3 Pin dimensions

The tool material is a proprietary CPM-1V tool steel alloy which exhibits good hardness and heat transfer properties. The properties of the model tool are same as that of actual tool but the model geometry does not include a recessed region around the pin or rounded edges. All these considerations are taken care of by assuming the weld material moving in the opposite direction instead of the tool in the forward direction which makes the modelling procedure unnecessary complicated. In this design, the tool is centered toward one end of the plate piece to allow the cooling material to be modeled. The various domains used in the model are indicated in Fig. 4.

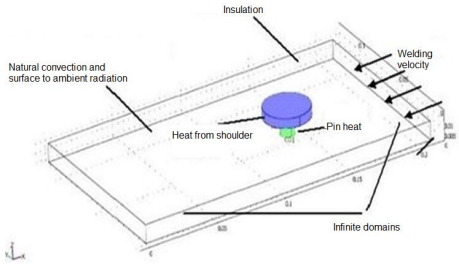

Fig. 4 Domains in the model geometry

The model dimensions are 0.210 m x 0.120 m x 0.010 m in positive x, y and z directions respectively. Aluminum alloy (AA6061-T6) is taken as the work piece due to its wide applications in the aerospace field because of its good formability, weldability, machinability, corrosion resistance and good strength compared to other aluminum alloys.

B. Governing Equations

The Navier-Stokes application for an incompressible fluid flow is followed to do the flow modelling. It is defined for a variable viscosity and constant density. The momentum balance equation is [11]:

$$\frac{\partial u}{\partial t} - \nabla \eta\left(\nabla u + (\nabla u)^T\right) + \rho(u.\nabla)u + \nabla p = F \quad (1)$$

which implies, (Accumulation of momentum per unit volume) – (Shear Stress) + (rate of momentum)+ (pressure forces) = (gravity forces); where, η =dynamic viscosity in kgm-1 s-1; u =velocity vector in ms-1; ρ =density of the fluid in kgm-3; P = pressure in Nm-2; F = body force term such as gravity.

The continuity equation for incompressible fluids is [11]:

$$\nabla.u = 0 \quad (2)$$

The modelling of the rotation of tool is done by following rotational velocity equations in x and y-axis. These equations are applied to boundaries between the tool face and aluminum plate:

$$u_{rot} = (-u\_weld) \times (y - y_{tool}) \quad (3)$$

$$v_{rot} = (-u\_weld) \times (x - x_{tool}) \quad (4)$$

The x and y velocity vectors are generated at every point (x, y) by these equations on the boundary which depends on the distance from the tool centre (x_{tool}, y_{tool}). This produces a rotating thin layer of aluminum i.e rotating with the same speed as that of the tool face. This motion spreads into the aluminum plate. Therefore, under a given viscosity, combining the effects of traverse speed and rotational speed, an internal velocity is generated.

Equation 1 constitutes the basic equation which has been used to analyse the steady state flow of incompressible fluid. In other words, the workpiece material has been idealized as a fluid. The material property correlating the flow stress and the strain rate is viscosity which is defined as:

$$\mu = \frac{\sigma_e}{3\dot{\varepsilon}} \quad (5)$$

where, σ_e is the effective stress or the flow stress as defined by:

$$\sigma_e = \frac{1}{\alpha}\sinh^{-1}\left[\left(\frac{Z}{A}\right)^{\frac{1}{n}}\right] \quad (6)$$

and $\dot{\varepsilon}$ is the effective strain rate, defined by;

$$\dot{\varepsilon} = A(\sin \alpha\sigma)^n \exp\left(\frac{-Q}{RT}\right) \quad (7)$$

where, Z is known as the Zener-Holloman temperature, Q is the temperature independent activation energy which is equal to self-diffusion energy, R is the gas constant, and α, A, and n are model constants which are determined by curve-fitting the test data obtained from [12] the hot extrusion of AA6061.

In the present model, the Carreau viscosity phenomenon is used as an alternative way to implement the nonlinear viscosity behaviour of the material. The Newtonian and Non-Newtonian laws have to be properly assigned to the model due to the existence of high strain rate and low strain rate around the tool pin and outside the TMAZ respectively which results in nonlinear viscosities. The Carreau model can fit in both Newtonian as well as non-Newtonian flow. It is defined by:

$$\eta = \eta_\infty + (\eta_0 - \eta_\infty)\left[1 + \left(\dot{\gamma}\lambda \exp\left(\frac{T_0}{T}\right)\right)^2\right]^{\frac{(m-1)}{2}} \quad (8)$$

where, η_∞ = infinite shear viscosity in kgm-1s-1; η_0 = zero shear viscosity in kgm-1s-1; $\dot{\gamma}$ = shear strain rate; λ = time constant; T_0= reference temperature in K; m= power law index for the non- Newtonian fluid.

Fitting this Equation with the analytical results for viscosity resolves the constants presented in the Carreau model. In this study, the constants are found to be η_0=1e8kgm-1s-1, η_∞=0, λ=10, T_0 = 300 K, and m = 0.

C. Grid Independence Study

The Comsol Multiphysics software is finite element package and hence the governing equations are discretised using finite element method. Due to this the meshing of the plate is done which divides the workpiece into small triangular elements. The grid points store the scalar variables that are surrounded by the control volume. The grid points also contains the vectors such as velocities, but are scattered with respect to the scalar variable to provide numerical stability in calculation. The material properties, weld parameters and tool and workpiece geometry are taken as input which gives velocity field as output. It is clear from the meshed workpiece as shown in Fig. 5 that finer grains are present near the tool which progressively becomes coarser away from the tool-shoulder periphery.

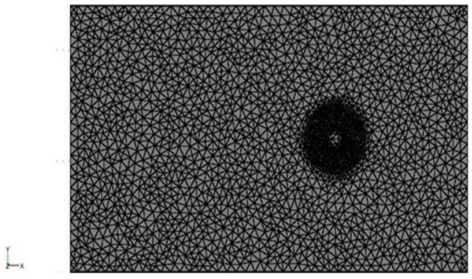

Fig. 5 A typical meshed workpiece for current observation

The mesh consisted of 19518 non-uniform triangular grid elements and 126163 total number of grid points. Also it was observed from Table I that the error in calculated minimum velocity remained almost constant and approximately zero when a fine mesh was used. So it can be said that mesh size between fine and finer must be chosen in order to have minimum error. Moreover, the program undergoes many numbers of iterations in the process to get the solution. The convergence of solution takes place in order to successfully solve the problem. In the present model, convergence is usually achieved within 400 iterations with a tolerance factor of 1e-6 which requires about 10 minutes in a PC with 2.10 GHz Intel(R) Core(TM) 2 Duo CPU and 3 GB of RAM memory.

TABLE I
EFFECT OF MESH REFINEMENT ON PREDICTED PROCESS VARIABLES

Mesh Modes	Velocity (ms-1)	Time Taken for simulation (s)	Percentage difference (Velocity) w.r.t extremely fine mesh
Coarse	0.29423147	354	0.69
Fine	0.3	576	0.72
Finer	0.3	941	0.72
Extremely Fine	0.29218826	1057	0

III. RESULTS

Based upon the model developed in the previous section, a detailed analysis of the material flow was performed. This is critical for AA 6061 T6 under different welding parameters. To decrease the computational time and keeping the accuracy of the model and obtain a reliable estimation of velocity of the flow, an FSW tool with a cylindrical pin and flat shoulder were assumed in the CFD model. The effect of different process parameters is described in following sections.

A. For Various Sticking Condition

The 2-D plot for streamlines of the velocity field is given in Figs. 6 (a)-(c). The lines show the paths that material particles follow from the inlet (opposite to the welding direction) to the outlet of the Eulerian region. The interesting features of the flow field occur close to the tool. Streamlines near the top and bottom boundaries exhibit almost straight paths. Near the tool, however reverses in the direction of flow occurs on the advancing side. A stagnation point, where velocity is zero, exists in the vicinity of the reversal point. Circular streamlines close to the tool pin indicate material region swept out by the pin. From 3D flow computations, it is possible to determine the path line of a material particle traced in the welding region. It is clearly seen that particles close to the pin undergo more than one rotation around the pin before being deposited. Also particles move from the retreating side to advancing side. Correlation between experimentally determined marker positions with numerical predictions can be useful in validation of flow models in FSW.

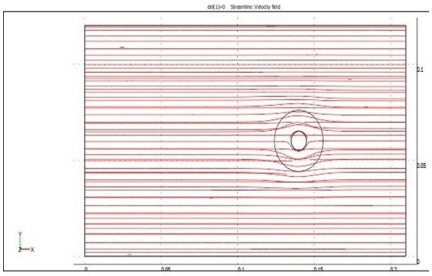

(a)

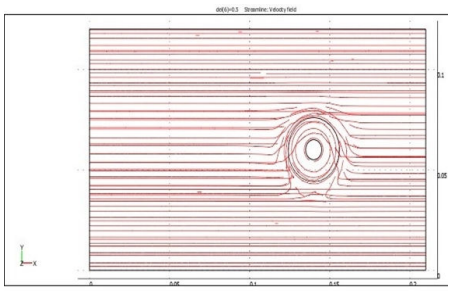

(b)

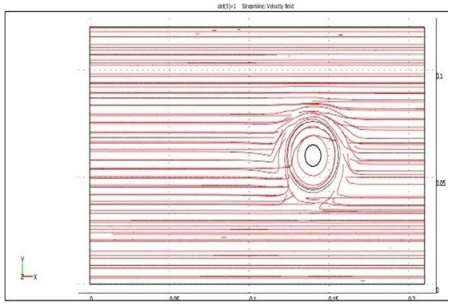

(c)

Fig. 6 Flow pattern for variable sticking condition, (a) sliding, (b) partial sticking/sliding, (c) full sticking for rotational speed of 400 rpm and welding velocity of 0.001 ms-1 and coefficient of friction 0.4

B. For Various Tool Traverse Speed

The streamline plot for various tool traverse speed of the tool can be seen in Figs. 7 (a)-(c). From the figure, it is clear that streamlines are organised for a higher tool traverse speed as compared to lower tool traverse speed. The flow lines are mostly oriented at higher welding speed giving a better material flow and perhaps a better output especially in terms of ultimate tensile strength.

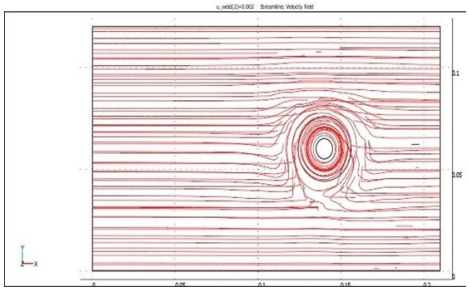

(a)

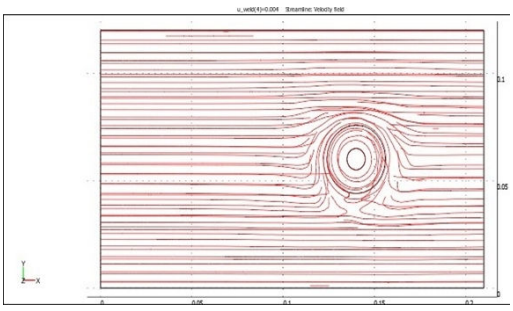

(b)

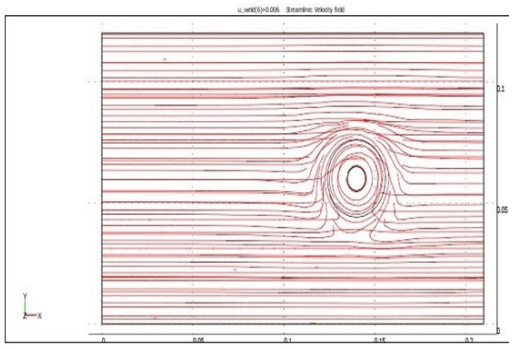

(c)

Fig. 7 Flow pattern for various tool traverse speed, (a) 0.002 ms-1, (b) 0.004 ms-1 and (c) 0.006 ms-1for rotational speed of 400 rpm, full sticking condition and coefficient of friction 0.4

C. For Various Rotational Speed

Figs. 8 (a)-(c) show an opposite nature of the streamline plot in connection to different tool rotational speed compared to those of different traverse speed. It is clear from the figures that flow pattern are mostly disoriented with an increase in rotational speed which may be due to excessive heat generation and increase in the sliding velocity of the shear layer underneath the shoulder and near to the tool periphery which may sometimes lead to spooling out of the material from the shoulder side thus increasing the depth of penetration.

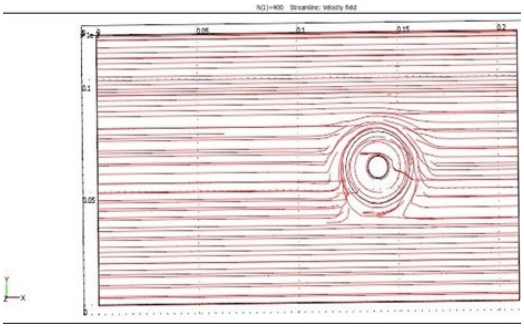

(a)

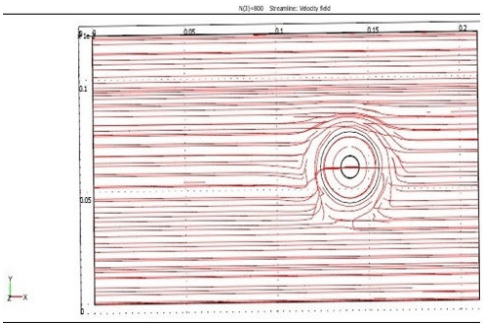

(b)

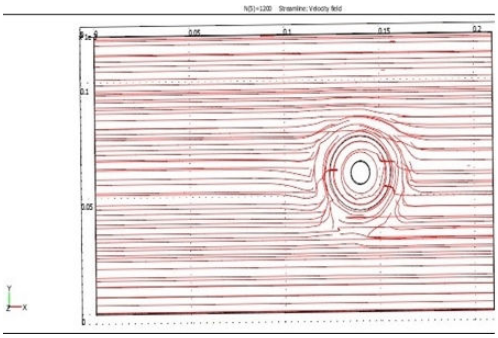

(c)

Fig. 8 Flow pattern for variable RPM, (a) 400 rpm , (b) 800 rpm, (c) 1200 rpm for welding speed of 0.001 ms-1, full sticking condition and coefficient of friction 0.4

D. Viscosity Variation

The variation in viscosity profiles along the shoulder with different sticking condition is seen in Figs. 9 (a)-(c). From Fig. 9 (a) it is clear that during full sliding condition viscosity is high in the vicinity of the shoulder and hence a small amount of material adheres to the tool and so proper material transfer does not take place. Whereas during full sticking condition as shown in Fig. 9 (c) the viscosity around the vicinity of the shoulder is very less and hence a large amount of material transfer takes place. An important consequence of the computed viscosity profiles is that high values beyond a certain critical value results in lack of plastic flow and hence defines the geometry of the Thermo-mechanically Affected Zone.

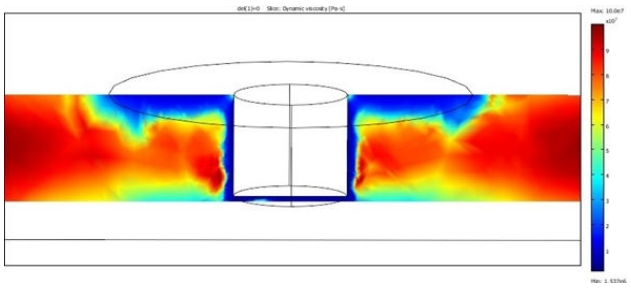

(a)

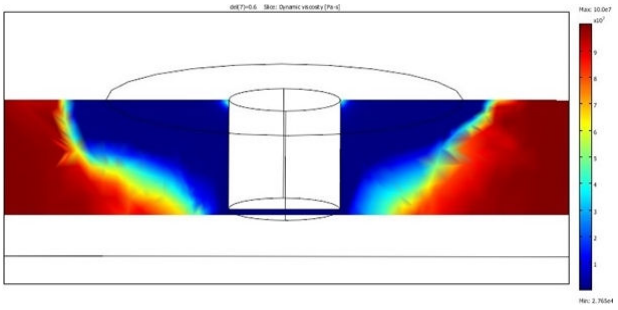

(b)

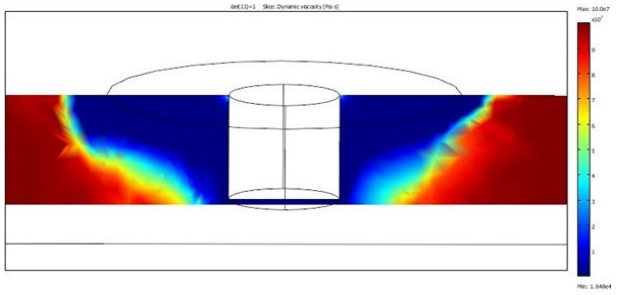

(c)

Fig. 9 Dynamic viscosity variation around the shoulder interface for, (a) full sliding, (b) partial sliding/sticking, (c) full sticking at a rotational speed of 400 rpm and tool traverse speed of 0.001 ms-1

The variation in dynamic viscosity around the pin can be seen in the sub-domain settings from the post processing menu of the solver. It is clear from the figures that effective viscosity decreases with the enhancement of the tool-material contact condition (Figs. 10 (a)-(c)).

Fig. 11 shows the variation of viscosity along the longitudinal i.e. x direction at different elevations, i.e., values of z. It is seen that at z= 0.010 m, viscosity decreases with increase in x followed by a sharp increase at high values of x.

Since the viscosity is inversely proportional to shear rate, the observation may be explained considering the values of strain rates presented in Fig. 13, where the shear rate trends are just opposite to those of the viscosity values presented here. At lower values of z, the viscosity progressively increases with x distance, which is also consistent with the shear rate variations.

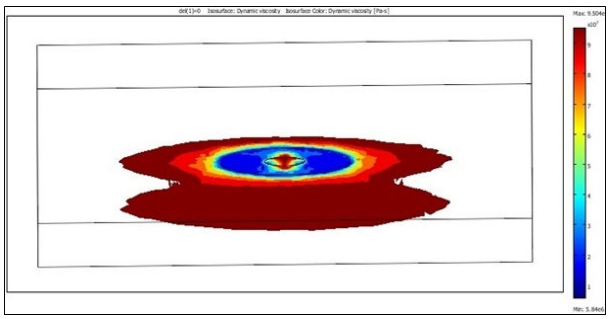

(a)

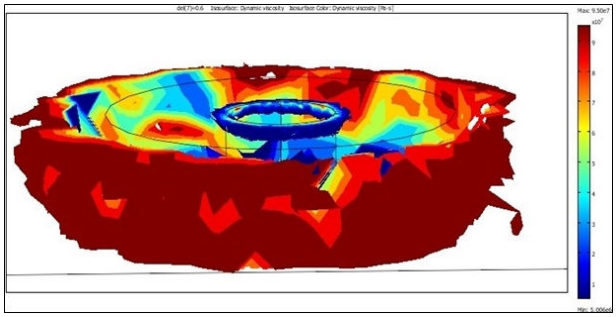

(b)

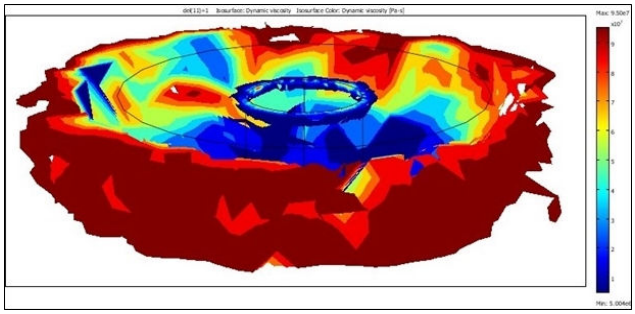

(c)

Fig. 10 Variation of viscosity around the pin for (a) sliding, (b) partial sliding/sticking, (c) sticking condition for rotational speed of 400 rpm and welding speed of 0.001 ms-1

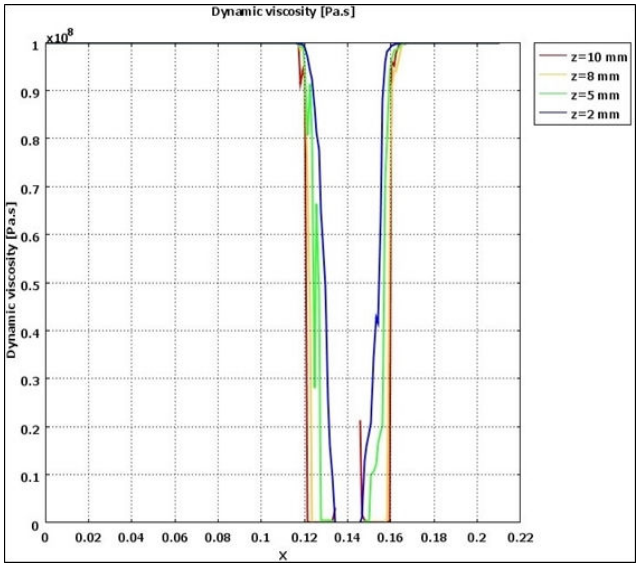

Fig. 11 Variation in dynamic viscosity around the shoulder interface at various depths of the pin

E. Shear Rate

The variation in shear rate on the shear layer beneath the shoulder and around the pin can be visualized from Figs. 12 (a)-(c). The figure shows that the maximum shear rate occurs near the surface of the pin where the maximum velocity gradient is present. For lower planes, shear rate rapidly

decreases with distance away from the tool axis. For higher planes, close to the shoulder, the velocity gradient decreases gradually away from the tool axis till below the shoulder periphery. Beyond the periphery, the velocity gradient decreases sharply because of the rapid decay of velocity.

Fig. 13 shows the computed shear rate behind the tool opposite to the direction of welding at different elevations in the AA6061-T6 workpiece. It is observed that shear rate decreases rapidly with depth, which may be attributed to large decrease in velocities away from the shoulder through viscous dissipation. In this case higher stain rates in the range of 250 s-1 has been calculated.

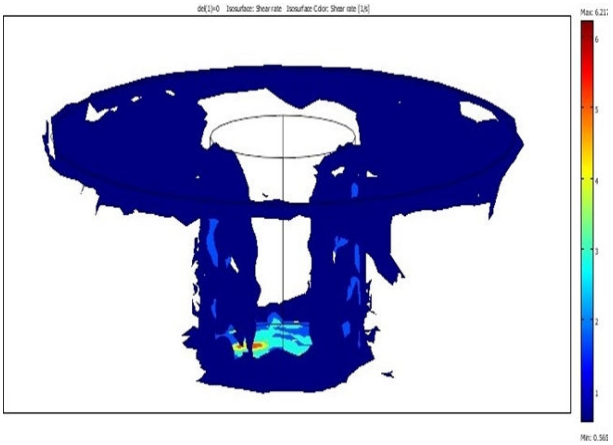

(a)

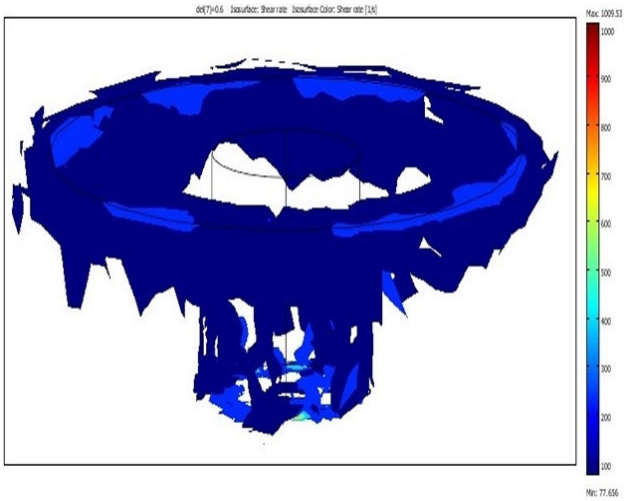

(b)

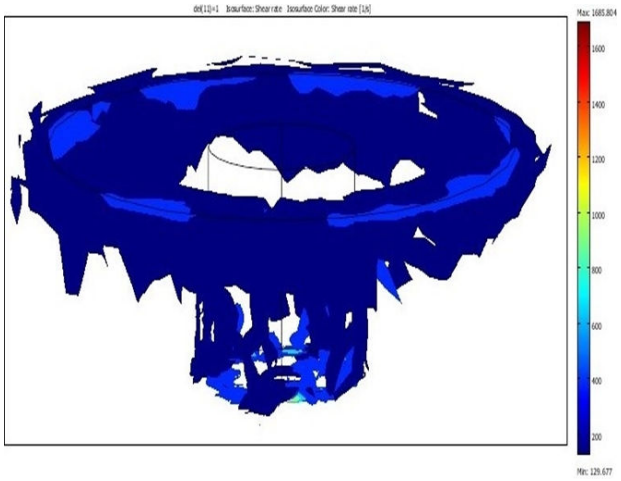

(c)

Fig. 12 Variation of shear rate for (a) full sliding, (b) partial sliding/sticking, (c) full sticking condition for rotational speed of 400 rpm and welding speed of 0.001 ms-1

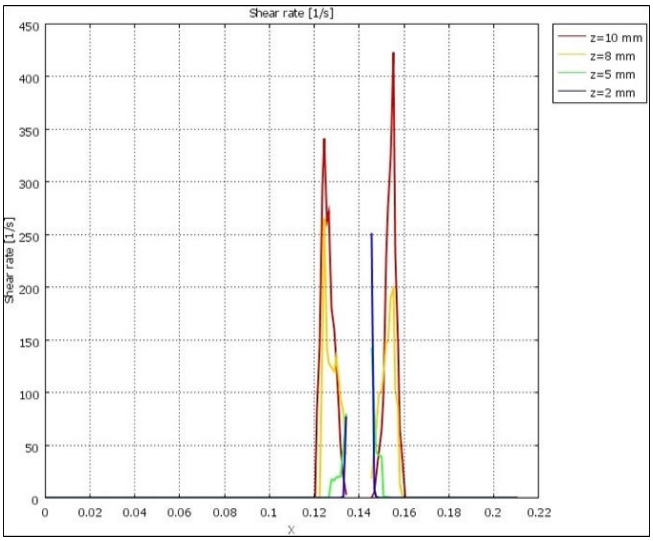

Fig. 13 Variation of shear rate around the shoulder at various depth of the pin

F. Velocity Field

The 2-D velocity plot shows the variation of velocity for different values of sticking conditions pertaining to AA 6061 workpiece (Figs. 14 (a)-(c)). It can be seen that as more material sticks to the pin with an increase in rpm, the velocity of the fluid particles close to the shoulder and the tool periphery increases within the Thermo- Mechanical Affected Zone and then decreases sharply where it assumes the normal inflow velocity of the material.

Figs. 15 (a)-(c) show the variation of velocity at different elevations i.e., z values for three different material contact condition. It is observed that at z = 0.010 m, velocity increases and attains a maximum at the outer periphery of the shoulder, i.e., at y = 0.044 m and 0.076 m (centre of the shoulder being

at 0.060 m) followed by a rapid decrease, while at planes near the bottom of the workpiece, the velocity peaks are attained at the tool surface. Here the value of slip was assumed constant. Therefore the highest value is at the shoulder periphery when velocity is greatest. Near the top surface, the effect of shoulder and the viscous momentum transfer is fairly pronounced resulting in high peak velocity. But since, momentum decays rapidly in the z direction away from the shoulder, the effect of rapid rotation of the shoulder do not reach the lower elevations.

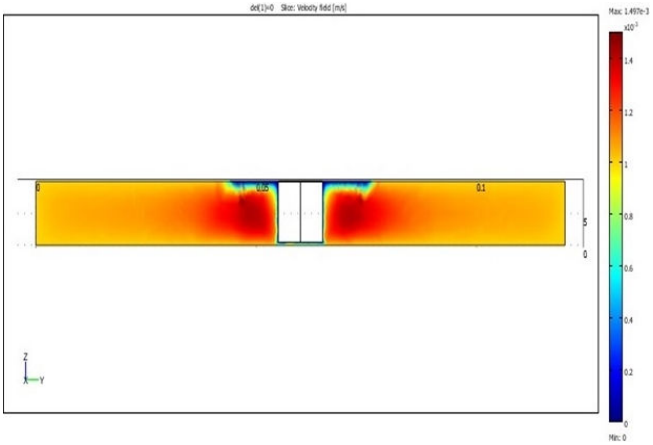

(a)

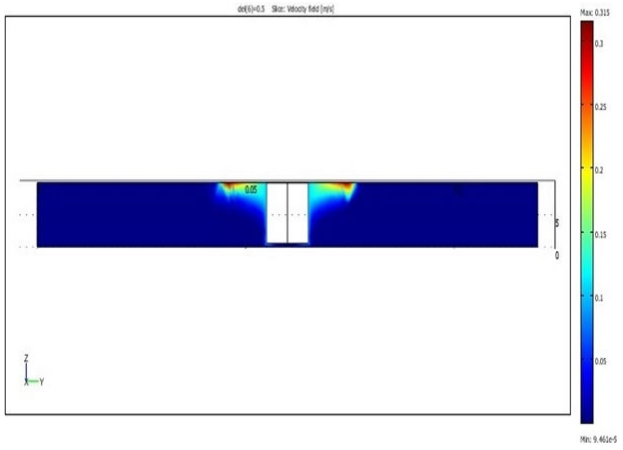

(b)

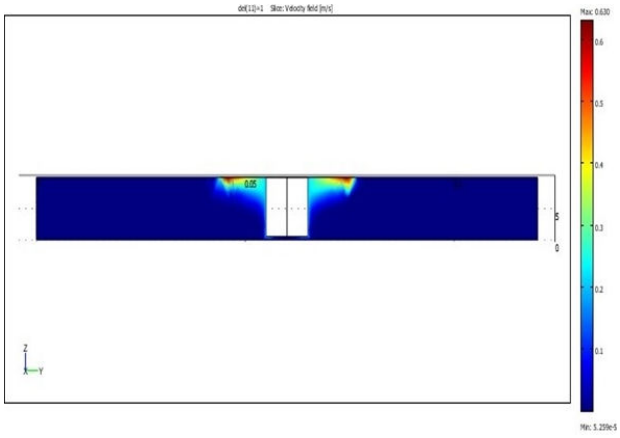

(c)

Fig. 14 Velocity profiles for (a) full sliding, (b) partial sliding/sticking, (c) full sticking condition for rotational speed of 400 rpm and welding speed of 0.001 ms-1

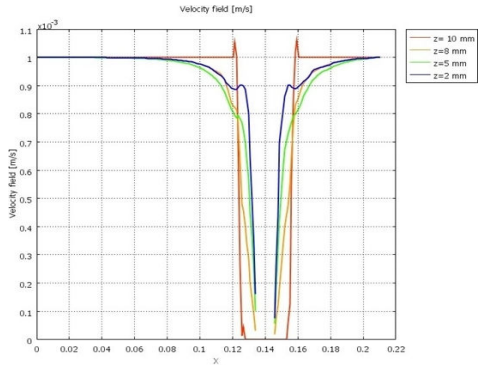

(a)

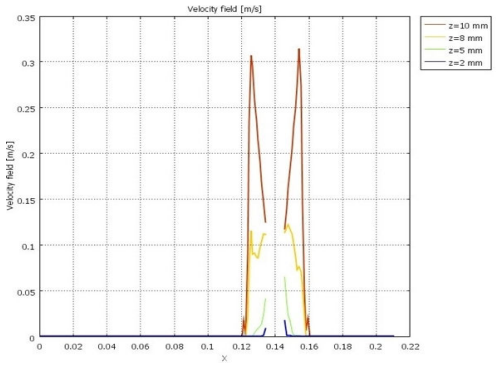

(b)

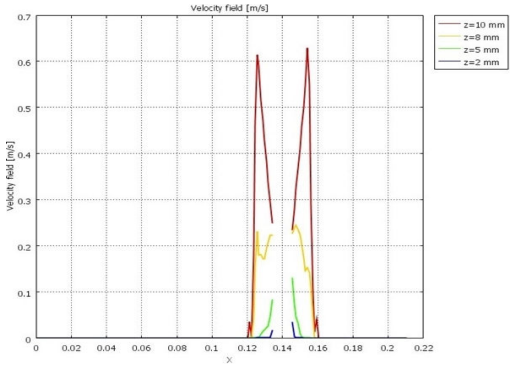

(c)

Fig. 15 Variation of velocity field in transverse and for various depths of the pin respectively for (a) full sliding, (b) partial sliding/sticking, (c) full sticking, for rotational speed of 400 rpm and welding speed of 0.001 ms-1

IV. Conclusion

A 3-D numerical analysis of material flow is presented for the butt FSW of AA6061-T6. The temperature-dependent material properties as well as the Carreau viscosity model are considered for the assumed visco-plastic material model. The CFD model is developed including the flat tool shoulder and a plain cylindrical tool pin. The 3-D plastic flow fields were predicted by solving the governing equations. The results showed significant material flow occurring near the tool. Circular closed streamlines are present near the tool pin which shows the presence of accumulated materials. The computed traces of streamlines also show that material flow mainly takes place in the retreating side. The optimum viscosity could be used to predict the shape of the thermo-mechanically affected zone. The tool geometry, rotational speed, contact condition between the tool-matrix interface and the change in thickness of the plate effects the strain rate significantly.

Acknowledgment

The Author would like to thank the Mechanical Engineering Department of National Institute of Technology Agartala for providing excellent opportunities in carrying out simulation based research work.

References

[1] W. M. Thomas, E. D. Nicholas, J. C. Needham, M. G. Murch, P. Templesmith, and C. J. Dawes, G. B. Patent Application 9125978.8, UK Patent Office, London,1991.
[2] R. Kovacevic, Welding Processes, *In Tech., (Chapter 9),* 2012.
[3] R. S. Mishra, and Z. Y. Ma, "Friction stir welding and processing", *Mater Sci Eng R*, 50, pp. 1–78, 2005.
[4] J. A. Schnieder, and A. C. Nunes, "Characterization of plastic flow and resulting micro textures in a friction stir weld", *Metallurgical and Materials Transaction*, 35(4), 777–783, 2004.
[5] Ulysse, P., 'Three-dimensional modelling of the friction stir-welding process', *International Journal of Machine Tools & Manufacture*, 42(14), pp. 1549–1557, 2002.
[6] H. Schmidt, and J. Hattel, "A local model for the thermomechanical conditions in friction stir welding", *Modelling and Simulation in Materials Science and Engineering*, 13, pp. 77–93, 2005.
[7] G. Buffa, J. Hua, R. Shivpuri, and L. Fratini, "Design of the friction stir welding tool using the continuum based FEM model", *Materials Science & Engineering A*, 419, pp. 381–388, 2006.
[8] K. Colligan, "Material flow behaviour during friction stir welding of aluminum", *Welding Journal,* Research Supplement, 78, pp. 229–237, 1999.
[9] T. U. Seidel, and A. P. Reynolds, "Visualization of the material flow in AA2195 friction-stir welds using a marker insert technique", *Metallurgical & Materials Transactions A*, 32, pp. 2879–2884, 2001.
[10] H. Schmidt, T. L. Dickerson, and J. Hattel, "Material flow in butt friction stir welds in AA2024-T", *Acta Materialia*, 54, pp. 1199–1209, 2006.
[11] H. B. Schmidt, and J. H. Hattel, "Thermal and Material Flow modelling of Friction Stir Welding using Comsol", Excerpt from the Proceedings of the COMSOL Conference, Hannover, 2008.
[12] J. A. Schneider, "Temperature Distribution and Resulting Metal Flow", Friction Stir Welding and Processing, *ASM International*, pp. 37-49, 2007.